Generation of a quasi-monoergetic proton beam from laser-irradiated sub-micron droplets

Generation of a quasi-monoergetic proton beam from laser-irradiated sub-micron droplets

S. Ter-Avetisyan, B. Ramakrishna, R. Prasad, M. Borghesi, P. V. Nickles et al.

Citation: Phys. Plasmas **19**, 073112 (2012); doi: 10.1063/1.4731712
View online: http://dx.doi.org/10.1063/1.4731712
View Table of Contents: http://pop.aip.org/resource/1/PHPAEN/v19/i7
Published by the American Institute of Physics.

Generation of a quasi-monoergetic proton beam from laser-irradiated sub-micron droplets

S. Ter-Avetisyan,[1,2] B. Ramakrishna,[1] R. Prasad,[1] M. Borghesi,[1] P. V. Nickles,[3,4] S. Steinke,[3] M. Schnürer,[3] K. I. Popov,[5] L. Ramunno,[5] N. V. Zmitrenko,[6] and V. Yu. Bychenkov[7]

[1]*Centre for Plasma Physics, School of Mathematics and Physics, The Queen's University Belfast BT7 1NN, United Kingdom*
[2]*ELI - Extreme Light Infrastructure, Institute of Physics, 18221 Prague, Czech Republic*
[3]*Max Born Institute, Nonlinear Optics and Short Pulse Spectroscopy, 12489 Berlin, Germany*
[4]*WCU Department of Nanobio Materials and Electronics, GIST, Gwangju 500-712, South Korea*
[5]*Department of Physics, University of Ottawa, Ottawa, Ontario K1N 6N5, Canada*
[6]*M. V. Keldysh Institute of Applied Mathematics, Russian Academy of Sciences, Moscow 125047, Russia*
[7]*P. N. Lebedev Physics Institute, Russian Academy of Sciences, Moscow 119991, Russia*

(Received 11 January 2012; accepted 24 May 2012; published online 20 July 2012)

Proton bursts with a narrow spectrum at an energy of (2.8 ± 0.3 MeV) are accelerated from sub-micron water spray droplets irradiated by high-intensity ($\sim 5 \times 10^{19}$ W/cm^2), high-contrast ($\sim 10^{10}$), ultra-short (40 fs) laser pulses. The acceleration is preferentially in the laser propagation direction. The explosion dynamics is governed by a residual ps-scale laser pulse pedestal which "mildly" preheats the droplet and changes its density profile before the arrival of the high intensity laser pulse peak. As a result, the energetic electrons extracted from the modified target by the high-intensity part of the laser pulse establish an anisotropic electrostatic field which results in anisotropic Coulomb explosion and proton acceleration predominantly in the forward direction. Hydrodynamic simulations of the target pre-expansion and 3D particle-in-cell simulations of the measured energy and anisotropy of the proton emission have confirmed the proposed acceleration scenario. © *2012 American Institute of Physics*. [http://dx.doi.org/10.1063/1.4731712]

I. INTRODUCTION

Laser-driven ion acceleration arises from the charge separation effects associated to the dynamics of relativistic electrons accelerated by the laser in the irradiated target region. Besides the intense-laser interaction with foil targets with thicknesses of several tens of microns up to a nanometre scale,[1,2] no other target concept could be demonstrated so far to be capable of proton emission with energies in excess of several tens of MeV. Additionally, up to now, an optimized laser target concept in terms of conversion efficiency cannot be given,[1] in spite of recent progress,[3] and it still requires an additional attention. Both high ion energies and conversion efficiencies are of vital importance for many foreseen applications,[4] which motivates further investigation of ion acceleration processes with different laser-target configurations.

Limited mass targets are of particular interest as the accelerated electrons confined within the small target volume may lead to an enhanced ion-accelerating field.[5,6] Recently, substantial increase of maximum proton energy and laser-to-ion energy conversion efficiency was measured when the surface of a foil target was reduced while keeping its thickness constant.[7] Sub-micron-droplets with a diameter $\sim$150 nm generated in a spray[8] are one kind of mass limited target from which MeV-protons[9] and quasi-monoenergetic proton bursts at 1.6 MeV have been measured.[10] The proposed acceleration scenario for these experiments was based on a combined thermal expansion[11]–Coulomb explosion (CE, Ref. 12) hybrid model, where three factors were playing a decisive role in achieving high proton energy: (i) favourable material composition (water), (ii) suitable droplet sizes resulting from droplet erosion by the low intensity pre-pulse, (iii) formation of an "iso-Coulomb-potential" distribution due to a substantial ionization of oxygen ions throughout the droplet volume. However, this scenario could not predict the asymmetric proton emission observed in the experiments, where the quasi-monoenergetic proton burst was accelerated in the forward direction.

This paper reports on the first experimental observation of a directional quasi-monoenergetic beam of protons at an energy of (2.8 ± 0.3) MeV from sub-micron objects (water spray of 150 nm droplets) irradiated by ultra-intense (5×10^{19} W/cm^2) and ultra-high contrast ($>10^{10}$) laser pulses. 3D particle-in-cell simulations allow to identify the acceleration scenario responsible for the observed increase of proton energy as compared to previous work[12] and for the anisotropy of the emission. In this scenario, the Coulomb explosion of the target is modified by the space charge of the confined electrons preferentially in the laser propagation direction causing an additional proton energy boost in the same direction.

II. EXPERIMENTAL SETUP

In the experiments,[10] a water spray target consisting of 150 ± 10 nm liquid droplets was irradiated by 40 fs, 1 J Ti:sapphire laser pulses at the High-Field-Laser-Application Laboratory of the Max-Born-Institute. With an f/2.5 off-axis parabolic mirror, an intensity of $\sim 5 \times 10^{19}$ W/cm^2 was achieved. The laser pulse was focused to a 5 μm spot (full width half maximum (FWHM)) at the centre of the spray[8]

with a radius ~1 mm in a steady flow of water vapour, 1 mm below the nozzle orifice. The laser pulse contrast, characterized by a third order autocorrelator with a dynamic range of 10^{12}, having a temporal resolution of 150 fs and a scanning range of ±200 ps, was below 10^{-8} at about 10 ps prior the main peak, where the pulse profile rises above the pedestal. The droplet density in the interaction region was 10^{11} cm^{-3}, the droplet diameter was (150 ± 10) nm, and the mean atomic density of the spray was of the order of 10^{18} cm^{-3}.

Two identical Thomson parabola spectrometers with absolutely calibrated micro-channel plate (MCP) detectors coupled to a phosphor screen have registered the ion spectra at the angles of 0° (laser propagation–forward direction) and 90° (transverse to the laser propagation direction)[13] emitted in a 70×10^{-9} sr solid angle. Each Thomson parabola spectrometer employed parallel 2 kV/cm electric and 0.27 T magnetic fields.

III. EXPERIMENTAL RESULTS

The ion energy spectra recorded in the forward and lateral directions are very different (Fig. 1). The selectivity and directionality of the acceleration mechanism is clearly seen by comparing the proton energy spectra along these directions (Fig. 1). A (2.8 ± 0.3) MeV quasi-monoenergetic proton beam has been measured only in the forward direction, while in the lateral direction the protons have much lower energy (~0.6 MeV) and exhibit a continuous spectrum. Oxygen ions with charges 1, 2, and 3 can be identified in the transverse direction while in the forward direction only O^{1+} can be seen clearly. It is interesting to note that the accumulated energy in the measured proton burst was deduced to be ~0.8 nJ, which seems to be higher than previous results.[10]

Asymmetric ion distribution can be measured in the experiments if both the protons are emitted in forward and lateral directions with different energies, or/and their spatial density distribution is not isotropic. According to the experimental conditions, one can exclude a modification of the protons spectra during their propagation through the spray (~1 mm radius). The stopping power of 100 keV protons in water is about 0.1 MeV·cm^2/mg,[14] while the average density in the spray is 0.03 mg/cm^3 or 10^{18} particles per cm^3. The proton mean free path is therefore much larger than the spray radius. In principle, the protons could collide with free electrons within the focal volume. However, the proton mean free path is much longer than the focal spot size due to the high electron temperature in the plasma, typically in the MeV-range. Correspondingly, proton scattering off free electrons is negligible.

In contrast, the propagation of oxygen ions through the spray is highly collisional.[15] Therefore, the measured Oxygen spectra are intrinsically asymmetric because the ions accelerated in the forward and backward directions have to propagate through the plasma channel created by the laser pulse, which ionizes and heats the water molecules, while in the lateral direction the ions propagate through cold and undisturbed medium. Hence, the free path lengths of the ions in the forward and lateral directions through the spray are quite different. This effect dominates and masks the initial

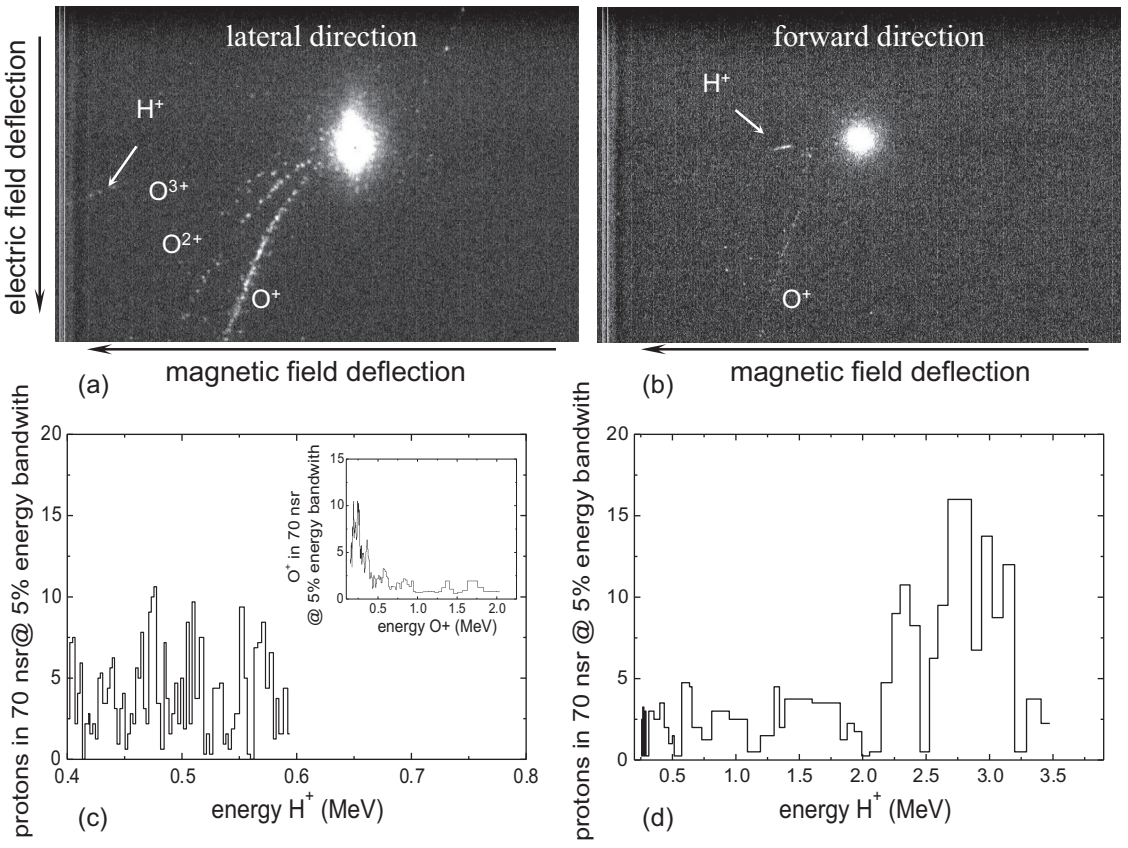

FIG. 1. Ion energy spectra emitted in lateral and forward direction.

angular emission profile of the ions accelerated within the focus volume in the spray.

IV. HYDRODYNAMIC SIMULATIONS OF TARGET PRE-EXPANSION

The process of laser interaction with the water droplet involves different stages due to the temporal profile of the laser pulse. Initially, the homogeneous spherical droplet interacts with the laser prepulse or pedestal. Deposition of the prepulse/pedestal energy into the droplet can result in its expansion, and consequently in the modification of the droplet density profile. The droplet can consist entirely of ionized water molecules and it can even collapse producing a gas target. Thus, the main pulse will be interacting with a target that is uniform in space and can have a size considerably larger and, consequently, a lower density than the initial droplet.

Measuring the evolution of the droplet modification is a challenging experiment. From the modelling point of view the entire evolution of the water droplet modification when laser intensity grows from $\sim 10^9$ W/cm^2 to $\sim 10^{12}$ W/cm^2 at ns time scale and then from $\sim 10^{12}$ W/cm^2 to $\sim 10^{15}$ W/cm^2 at ps time scale requires ns-long hybrid simulations of multi-species hydrodynamics, Multi-phase absorption, diffraction, scattering, and ionization should be adequately described. However, for a basic understanding we have set aside such complicated modelling and, by using the code DIANA,[22] have performed a simplified spherically symmetric one-fluid hydro-simulation of target expansion on a $\sim$10 ps time scale prior to the main pulse. The code DIANA includes equation of state with cold and thermal parts, collisional (inverse bremsstrahlung) absorption, two-temperature approximation (electrons and ions) with electron and ion heat conductivities, and volumetric radiation losses. Non-equilibrium averaged-charge kinetics include three processes: ionization by the electrons, photo recombination, and triple recombination as given in Ref. 23.

The initial incident laser intensity into the target is about 10^{12} W/cm^2 at 10 ps before the pulse peak and increases linearly in time during the simulation. The initial mass density of the 150 nm-diameter droplet target is 1 g/cm^3, the electron temperature is 10 eV, ions are at room temperature, and the average (effective) ion charge is $\langle Z \rangle = 0.49$. The heat of sublimation, the sound speed, and the Gruneisen constant are 2.6×10^{10} erg/g, 1.2 km/s, and 1.87, respectively. The dynamics of the target expansion is illustrated in Fig. 2.

In the beginning ($t < 6$ ps), an ablation pressure gives rise to a compression wave in the droplet. Ablation with the velocity 14-15 km/s produces a compression of the central

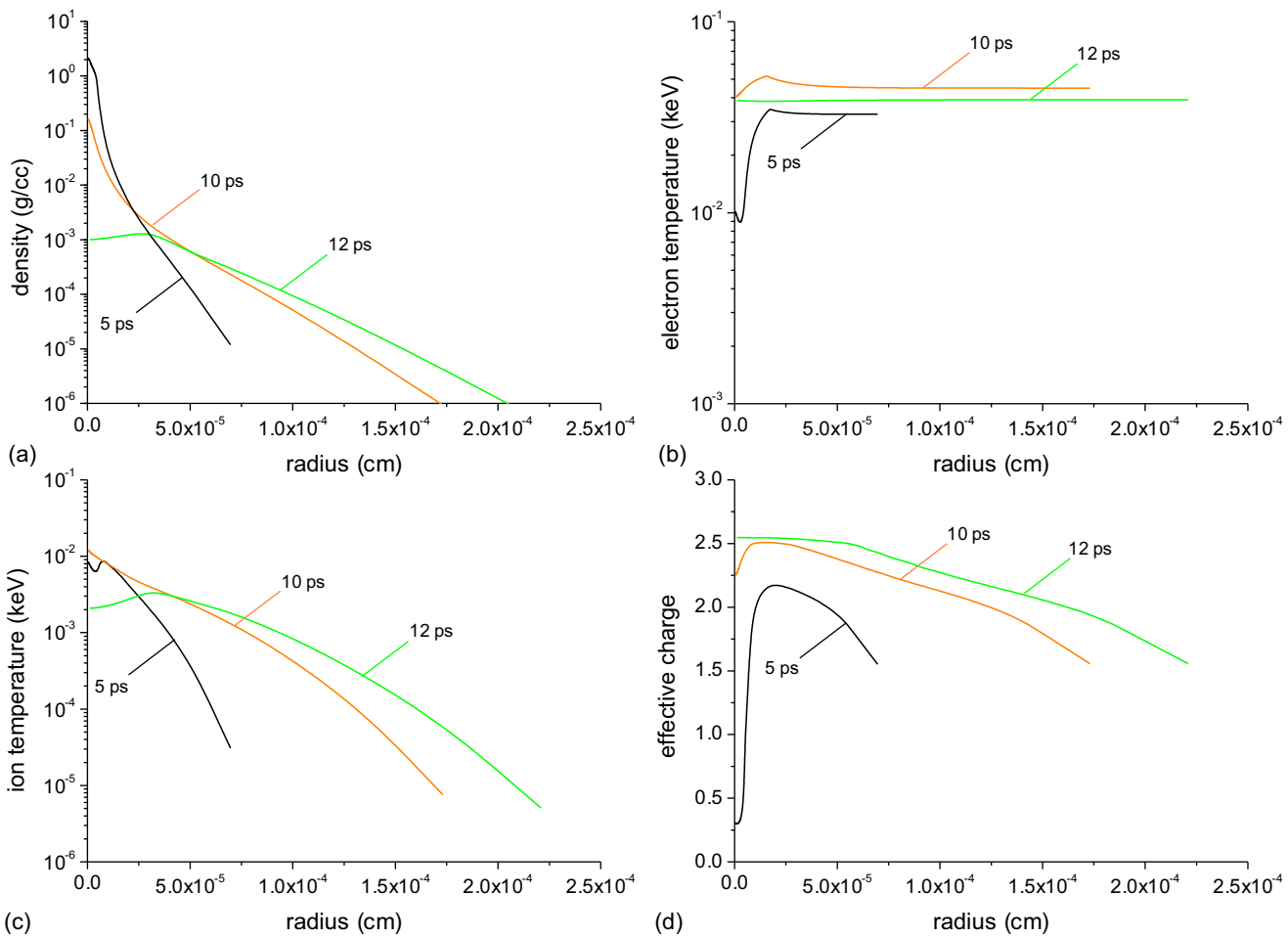

FIG. 2. The radial distribution of the mass density (a), electron temperature (b), ion temperature (c), and effective charge (d) at the hydrodynamic stage of droplet expansion.

part of the droplet up to $2\,g/cm^3$ at 4–6 ps. The maximum compression ($2\,g/cm^3$) is reached at the instant ~5 ps when the pressure is approximately 4 Mbars and temperature is 8–10 eV. After 6 ps, only expansion of the droplet takes place. Fig. 2(a) demonstrates the density decrease of the droplet and its effective radius increase within the characteristic time scale of few ps. At the beginning, the electron temperature grows and then decreases due to adiabatic cooling (Fig. 2(b)), while the ion temperature does not increase (Fig. 2(c)). The effective ion charge reaches $\langle Z\rangle = 2.5$ (Fig. 2(d)) which is rather close to the maximum value of 3.3. The simulation shows expansion of the whole droplet after ~12 ps, when laser intensity is still $\sim 10^{13}\,W/cm^2$. The droplet shape used in particle-in-cell (PIC) simulations matches qualitatively the shape in Fig. 2(a) at 10 ps. At longer times, hydrodynamic expansion (i.e., at higher laser contrast intensity) the target is completely vaporised and the main pulse interacts with gaseous target in the focal volume.

For full penetration of the laser pulse inside the droplet, a full ionisation by the high peak laser field of both hydrogen and oxygen atoms takes place.[16] In this case, the electron density inside the droplet reaches $n_{e,max} = (8+2)N_A\rho_\mu/M_\mu \approx 3.3\times 10^{23}\,cm^{-3} \approx 200\,n_{cr}$, where n_{cr} is the critical electron density at $\lambda = 800$ nm laser wavelength, N_A–Avogadro number, ρ_μ is mass density, and M_μ is the molar mass of water. The relativistic skin depth is $\delta_r \sim \gamma c/\omega_{pe}$ (where γ is the relativistic factor of electrons estimated through the dimensionless laser field amplitude a as $\gamma \approx a^2/2 \approx 12$ for linearly laser polarization and ω_{pe} is the electron plasma frequency) which can be estimated as: $\delta_r \sim \gamma\lambda/(2\pi\sqrt{n/n_{cr}}) = \gamma\lambda/(2\pi\sqrt{200}) \approx 100$ nm. Therefore, we assume full laser penetration into entire droplet. As the target size increases due to the pre-heating by the laser prepulse, its maximum density decreases that again validates our assumptions.

The interaction of an intense ($5\times 10^{19}\,W/cm^2$) linearly polarized laser pulse, with temporal (FWHM of $\Delta T_{FWHM} = 45$ fs) and spatial (FWHM of the focal spot of 3 μm) Gaussian profile, with the spherical H_2O plasma target and the subsequent target explosion are simulated using a 3D electromagnetic PIC code SCPIC.[17] The total energy in the laser pulse is about 1 J. We refer to the plane specified by laser polarization vector and beam axis as the P-plane and to the plane perpendicular to the beam axis at best focus as the S-plane.

V. RESULTS OF PARTICLE-IN-CELL SIMULATIONS

A. Laser interaction with an unmodified droplet target

At an infinite laser pulse contrast the high intensity laser pulse interacts with a 150 nm plasma sphere with a uniform density distribution of 200 n_{cr}. In the simulations, we used a rectangular grid with 130^3 points per λ^3 and $24^3 \approx 1.4\times 10^4$ particles per cell.

PIC simulations have demonstrated that the strong field of the laser pulse is capable of removing almost all the electrons from the droplet that escape leaving behind a positively charged sphere which undergoes a Coulomb explosion. The plasma charge density distributions in the two perpendicular S- and P-planes are shown in Fig. 3.

The explosion is characterized by formation of a proton shell moving out from a relatively slow expanding core of oxygen ions. The expansion is to a high extent spherically symmetric and follows a well-studied Coulomb explosion scenario of two ion species target.[18–21] The proton emission spectra in the forward and lateral directions are almost identical with a cut-off energy $\varepsilon_{max} \sim 5$ MeV (Fig. 4) which is close to the theoretical maximum value (~7.1 MeV, Ref. 20) for a Coulomb explosion of a fully ionised 150 nm water droplet.

Since the spectra in Fig. 4, that are typical for Coulomb explosion of unmodified sub-wavelength targets, disagree with the experimental results (Fig. 1), one may guess that the target modification during the interaction with the laser pulse pedestal plays a vital role toward the strongly asymmetric proton emission observed in the experiment.

B. Laser interaction with a modified droplet target

To account for a droplet modification during the interaction by the "low" intensity ps laser prepulse preceding the high intensity peak, we use the *ad hoc* hypothesis that the

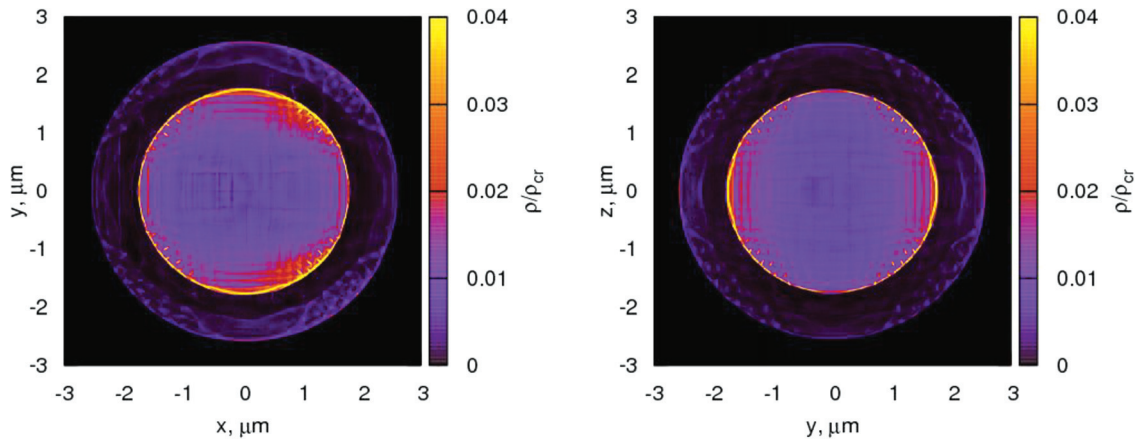

FIG. 3. Charge density distribution of an exploding 150 nm droplet (with initially homogeneous density) in the S and P-planes ~70 fs after the peak of the laser pulse has passed through the target centre. The laser pulse propagates in the $+\hat{x}$ direction. The laser field is polarized along the $\hat{y}$ axis. Ion bi-partition onto spherical heavy ion core and thin proton shell is clearly seen.[18–21]

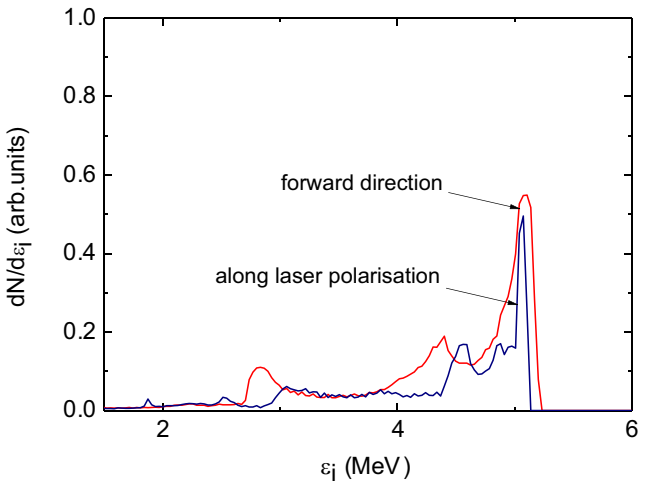

FIG. 4. Proton spectra in the forward direction and along the laser polarization direction (lateral direction) originated from laser interaction with initially homogeneous 150 nm droplet.

pre-heating of the droplet significantly increases its size, and the charged density distribution of the expanded droplet has a Gaussian shape which coincides with the mass density distribution. This hypothesis is partially supported by our previous simulations of adiabatic hot-electron-driven expansion of plasma into vacuum[21] and by the simplified hydrodynamic simulation presented above. The results following from such approach are qualitative, but they help to understand the physics of the forward-to-side accelerated proton energy anisotropy.

Another issue that must be taken into account is that in the experiments one has a spray of droplets rather than a single droplet. This can possibly result in a number of competing phenomena influencing the laser propagation (scattering or self-focusing) and causing additional macro-fields (electrostatic fields and quasistatic magnetic fields in the focal domain). To account for them, we have considered three cases: (a) maximum laser intensity $I_{max} = 5 \times 10^{19}$ W/cm^2, with the spot size (FWHM) 3 μm, called nominal case; (b) $I_{max} = 1.1 \times 10^{20}$ W/cm^2, FWHM = 2 μm, self-focusing case; (c) $I_{max} = 1.8 \times 10^{19}$ W/cm^2, FWHM = 5 μm, defocusing case. At first, we are neglecting the presence of neighbouring droplets and the influence of the collective electrostatic and magnetostatic fields of the surrounding droplets on the electrostatic field inside the expanding droplet. The mutual effect of the neighbouring droplets is discussed separately in the Subsection V C of this chapter.

We used the initial electron density profile in a plasma droplet in the form:

$$n_e(r) = 200 n_{cr} \cdot \frac{4}{3\sqrt{\pi}} \left(\frac{r_0}{r_g}\right)^3 \exp\left[-\left(\frac{r}{r_g}\right)^2\right], \qquad (1)$$

where r_0 is the radius of the droplet and r_g is the Gaussian radius of the pre-expanded droplet. Because of a smaller plasma density in the pre-expanded target compared to the unmodified droplet, in the simulations we used a smaller resolution ($\sim 40^3$ mesh points per λ^3) and number of particles per cell ($\sim 10^2$). The proton cut-off energy in the forward direction and forward-to-side energy ratios vs. r_g are shown in Figs. 5(a) and 5(b), respectively, for the nominal, self-focusing, and defocusing intensity cases. The pre-expanded target is capable of producing non-negligible proton energy anisotropy when the droplet size exceeds ~300 nm. Under these conditions, both the cut-off energy and energy anisotropy depend on the laser intensity. This is in contrast to smaller droplets ($r_g < 300$ nm), where the proton energy is isotropic and is almost independent from the laser peak intensity. The proton energy anisotropy is ~2 for 75 nm droplets pre-expanded to $r_g = 350$–450 nm (Fig. 5(b)). However, the maximum proton energy reaches only ~2.2 MeV (Fig. 5(a)), which is less than the values measured in the experiment (Fig. 1).

To overcome this inconsistency between the simulation and experimental result for maximum measured proton energy, we have considered also slightly larger droplet having $r_0 = 90$ nm, assuming possible fluctuations of the droplet size in the spray. The maximum proton energies and forward-to-side energy ratios as a function of the droplet size are shown in Figs. 5(c) and 5(d). The proton spectra in forward and lateral directions from the pre-expanded sphere of $r_g = 400$ nm irradiated by a 5×10^{19} W/cm^2 pulse (nominal case) are shown in Fig. 6. The spectrum demonstrates considerable forward-sideward anisotropy (~2) in both proton energies and number of particles.

It is expected that the emission anisotropy is a result of asymmetric field distribution around the droplet established by the electrons which are mostly driven along the laser propagation direction in the case of a pre-expanded target. Indeed, at an intensity of 5×10^{19} W/cm^2 the electron dynamics from an unmodified solid-density target and from a pre-expanded target is significantly different (Fig. 7). The electrons are driven from the pre-expanded target as an electron cloud (Fig. 7(a)) with a lateral size comparable to the target size, while in the case of an unmodified target the electrons form two trains of small-sized attosecond bunches seen in Fig. 7(b) (cf. Ref. 17). These attosecond trains propagate with angular divergence depending on the laser intensity, but almost do not affect the ion explosion isotropy (see Figs. 3 and 4). This is a result of the small size of bunches whose electrostatic field becomes negligible compared to the field of the ion core as soon as the bunches are displaced by a distance of the order of target size from the droplet. In contrary, the anisotropic electrostatic field generated by the electrons leaving the pre-expanded target changes considerably more slowly as they are extracted from the target, due to the much larger size of the electron cloud. The ions respond to this field, which results in the target elongation in the longitudinal direction (Fig. 7(c)). At later times, the deformed target experiences a non-isotropic Coulomb explosion (Fig. 7(d)) that results in a preferential direction of proton emission (Fig. 6).

C. Laser interaction with water spray target

The average distance between the individual droplets in the spray that has a density ~10^{11} droplet/cm^3 is about 2.2 μm which is comparable to the size of pre-expanded

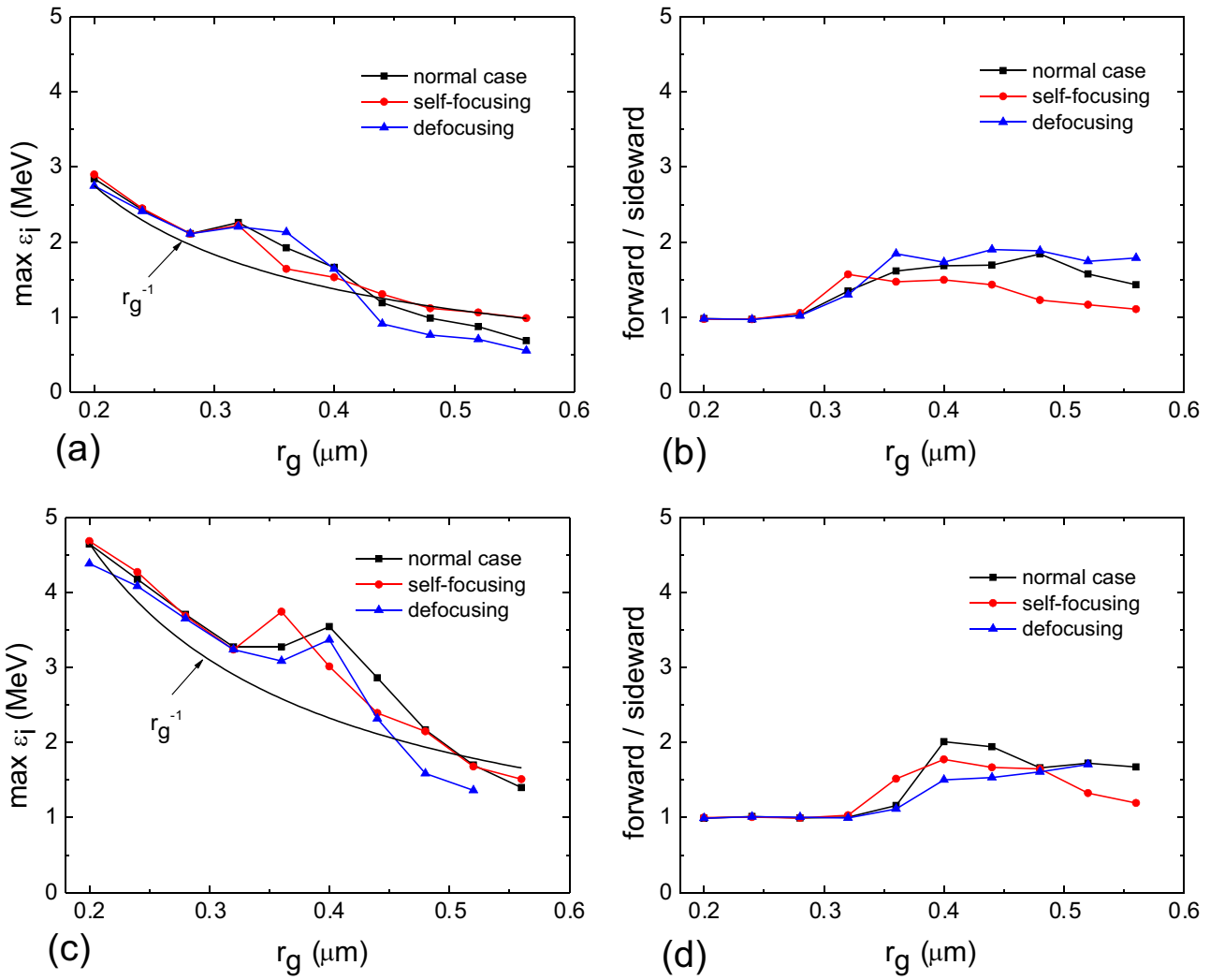

FIG. 5. Proton cut-off energy in the forward direction (a), (c) and forward-to-side cut-off energy ratio (b), (d) for a target with initial distribution (1) with $r_0 = 75$ nm (a), (b) and $r_0 = 90$ nm (c), (d). Solid lines: nominal case; dashed lines: self-focusing; dotted lines: defocusing. Sideward direction is considered along the laser polarization.

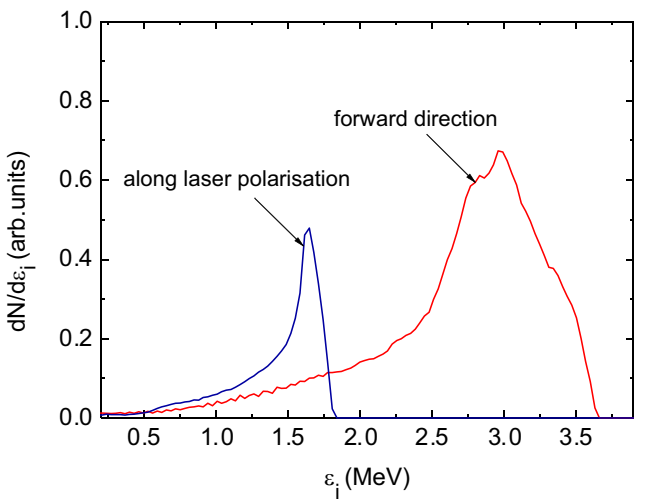

FIG. 6. Proton spectra in the forward direction and along the laser polarization direction from a 90-nm water droplet pre-expanded to a Gaussian sphere of radius 400 nm, irradiated by a pulse of intensity 5×10^{19} W/cm^2.

droplet (0.4 μm). Therefore, it is possible that the superposition of the fields of adjacent droplets can change the spatial and spectral characteristics of the protons and, in particular, the peak formation in proton spectrum can be affected. To analyse these changes and account for interaction between the neighbouring droplets in the focal volume, we have performed PIC simulations with two droplets. In these simulations, the distance between the centres of pre-expanded droplets was set 2 μm. One droplet (called "test droplet") was placed exactly at the laser focus and the other right behind on the line of laser beam axis: 0°, and at the angles 45° and 90° in respect to the laser beam axes.

The spatial particle density distribution for exploding droplets positioned at 45° with respect to the laser beam axis at about 250 fs after the peak of the pulse has passed through the test target centre is shown in Fig. 8(a). The proton spectra from the "test droplet" collected in a 2° cone angle in forward and along laser polarization (lateral) directions are depicted in Figs. 8(b) and 8(c), respectively, for different arrangements of the droplets.

As one can see from Fig. 8, the field of neighbour droplets may screen the accelerating field of the "test droplet"

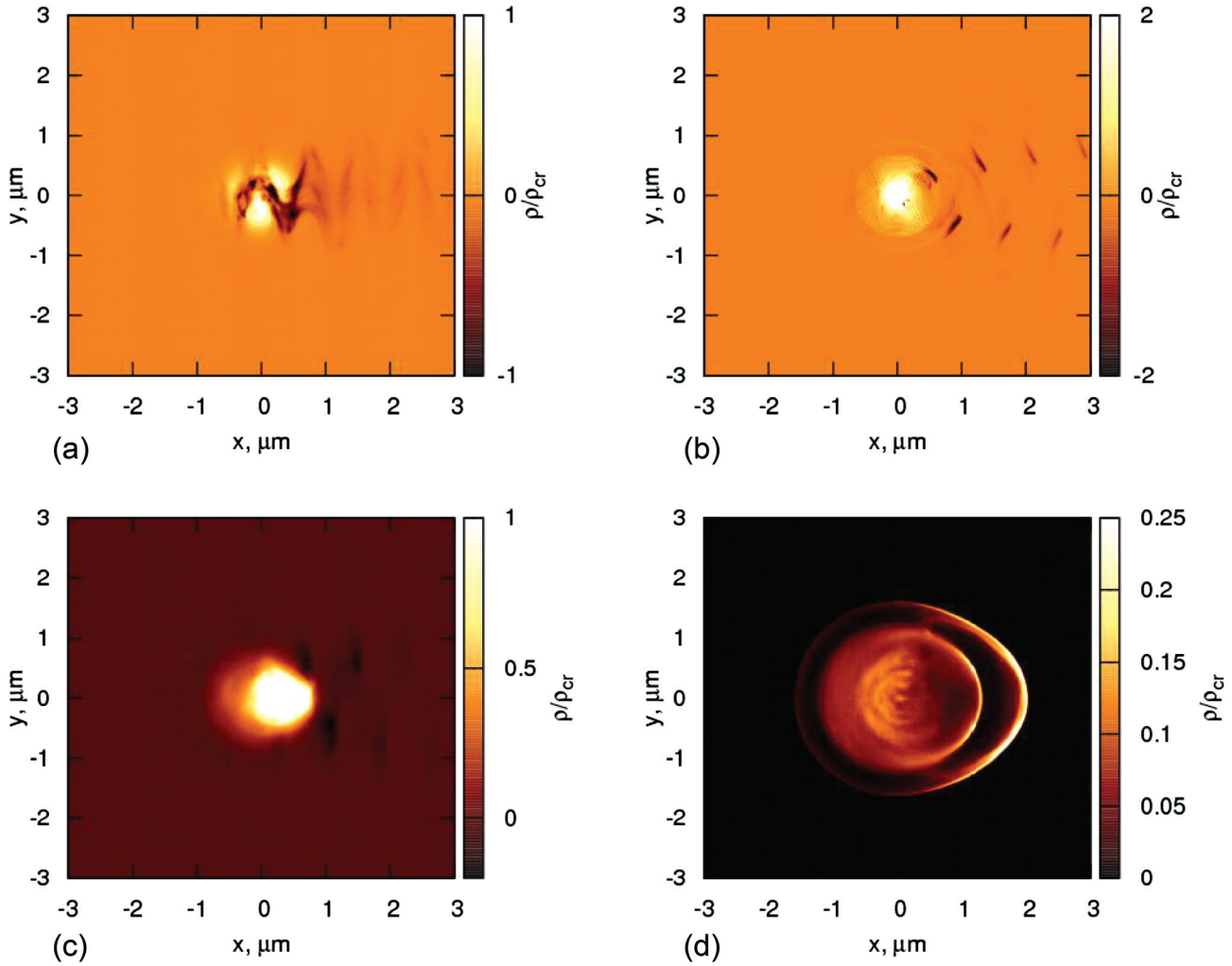

FIG. 7. Charge density distribution at different stages of interaction. (a), (b) electron extraction from a pre-expanded (a) and unmodified (b) water droplets of radius 90 nm; (c) charge density profile of the pre-expanded target ~30 fs after the top of the pulse has passed through the target centre; (d) charge density profile of the pre-expanded target during the Coulomb explosion stage (~165 fs after the top of the pulse has passed through the target centre).

depending on their relative disposition (compare Figs. 8(b) and 8(c)). However, ~3 MeV as a possible maximum energy along the laser beam is a reasonable estimate because of the probabilistic nature of the droplet distribution in the spray. In the lateral direction (Fig. 8(c)), some specific droplet position arrangement may lead to 2 MeV protons (at 0°), whereas the most probable energy is in the range of ~1 MeV.

Similarly, the shot-to-shot variations of the proton peak energy observed in the experiments are mainly caused by the fluctuations of the droplets distribution in the spray. The

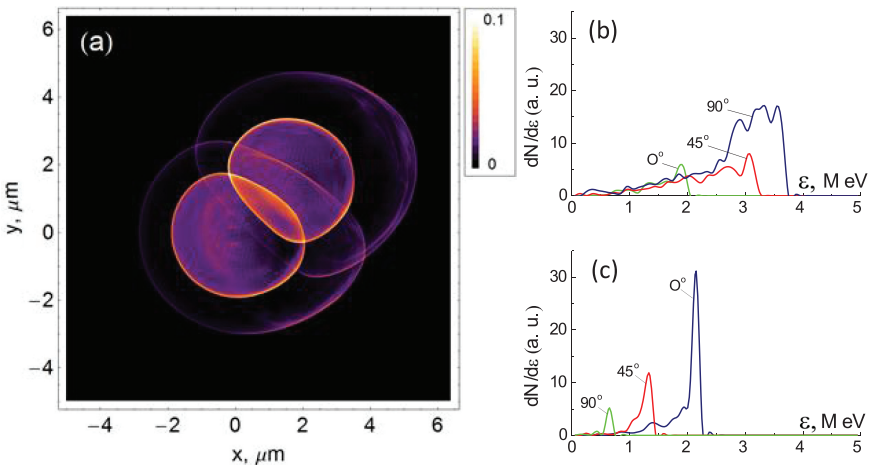

FIG. 8. (a) Space distribution for exploding droplets positioned at 45° in respect to laser beam axes at about 250 fs after the top of the pulse has passed through the test target centre. The proton spectra from "test droplet" collected in a 2° cone angle in (b) forward and (c) along laser polarization (lateral) directions are shown at 0°, 45°, and 90° disposition of the droplets relative to laser axes.

measured statistics shows that the influence of other possible sources on the proton peak energy variations, such as uncontrolled prepulse variations on a few ps timescale and fluctuation of amplified spontaneous emission (ASE) pedestal (with typical fluctuations less than a factor of 3) is much less significant than the droplets distribution fluctuations between different laser shots.

Additionally, the electrostatic charge separation macrofield which may appear in the caustics of the focus due to ponderomotively driven electrons away (radially) from the droplets is also negligible. Indeed, the charge separation field due to the ponderomotive force is estimated to be of the order of 10^{11} V/m. This field is maximum at the plasma channel boundary (at about 2–2.5 μm from the centre) and acts no longer than 100 fs (because the laser pulse duration is 40 fs). Hence, a proton may gain a maximum additional momentum in such radial field ~0.005 mc (2 MeV proton has momentum 0.03 mc) which can be disregarded.

At last, a possible magnetic field in the focal domain maybe important if $\omega_{ci} \sim u_i/l_R$, where ω_{ci} is the ion cyclotron frequency, u_i is the velocity of accelerated ions, and l_R is the Rayleigh length. This would require the magnetic field strength of almost 100 MG, but that is far from reality for gaseous plasma at the intensity of the experiment.

D. Laser interaction with a gaseous target

We have also performed PIC simulations when the target is completely vaporised and the main pulse interacts with a gaseous target in the focal volume. It was found that the maximum proton energy do not exceed 100 keV. This practically confirms the chosen target shape to simulate the experimental measurements.

VI. CONCLUSIONS

This letter reports on experimental observations of quasi-monoenergetic bursts of protons with energies of about ~3 MeV from sub-micron water droplets irradiated by ultra-intense (5×10^{19} W/cm^2) and high contrast ($>10^{-8}$) laser pulses. This is the highest energy, quasi-monoenergetic proton beam observed in a laser plasma experiment so far. The proposed scenario confirmed by hydrodynamic simulations and 3D particle-in-cell simulation allowed to identify the processes responsible for both the observed increase of proton energy and the anisotropy of emission. Based on the comparison between targets of different sizes (Fig. 5), we can also predict that the proton energies can be further increased if bigger droplets are used. In particular, based on a simple electrostatic model of Coulomb explosion, the maximum proton energy scales approximately as

$$\varepsilon \propto R\sqrt{\delta_r \cdot (Zn_i + n_p)},$$

where R is the target radius, δ_r is the skin depth, n_i is the density of heavy ions, Z is their charge, and n_p is the proton density. This scaling holds as long as the laser is capable of removing the majority of electrons from the target. In this way, the interaction of a high contrast laser pulse, focused to the diffraction limit, with a high-Z droplet can be advantageous for maximizing the proton energy.

ACKNOWLEDGMENTS

This research was supported by Laser Lab Europe proposal MBI001668, ELI-Beamlines (CZ.1.05/1.1.00/483/02.0061), Transregio18 (DFG), EPSRC Grants No. EP/E035728/1 (LIBRA Consortium) and No. EP/F021968/1, and Russian Foundation for Basic Research (Grant Nos. 10-02-91060-NCNI, 11-01-00267a, and 12-02-00231a). P.V.N. acknowledges the support of the World Class University program (R31-2008-000-10026-0) grant provided by National Research Foundation (NRF) of Korea.

[1]R. Prasad, A. A. Andreev, S. Ter-Avetisyan, D. Doria, K. E. Quinn, L. Romagnani, C. M. Brenner, D. C. Carroll, N. P. Dover, D. Neely, P. S. Foster, P. Gallegos, J. S. Green, P. McKenna, Z. Najmudin, C. A. J. Palmer, J. Schreiber, M. J. V. Streeter, O. Tresca, M. Zepf, and M. Borghesi, Appl. Phys. Lett. **99**, 121504 (2011).
[2]D. C. Carroll, O. Tresca, R. Prasad, L. Romagnani, P. S. Foster, P. Gallegos, S. Ter-Avetisyan, J. S. Green, M. J. V. Streeter, N. Dover, C. A. J. Palmer, C. M. Brenner, F. H. Cameron, K. E. Quinn, J. Schreiber, A. P. L. Robinson, T. Baeva, M. N. Quinn, X. H. Yuan, Z. Najmudin, M. Zepf, D. Neely, M. Borghesi, and P. McKenna, New J. Phys. **12**, 045020 (2010).
[3]A. V. Brantov, V. Yu. Bychenkov, K. I. Popov, R. Fedosejevs, W. Rozmus, and T. Schlegel, Nucl. Instrum. Methods A **653**, 62 (2011).
[4]M. Borghesi, J. Fuchs, S. V. Bulanov, A. J. Mackinnon, P. K. Patel, and M. Roth, Fusion Sci. Technol. **49**, 412 (2006).
[5]S. Karsch, S. Düsterer, H. Schwoerer, F. Ewald, D. Habs, M. Hegelich, G. Pretzler, A. Pukhov, K. Witte, and R. Sauerbrey, Phys. Rev. Lett. **91**, 015001 (2003).
[6]S. Ter-Avetisyan, M. Schnürer, P. V. Nickles, M. Kalashnikov, E. Risse, T. Sokollik, W. Sandner, A. Andreev, and V. Tikhonchuk, Phys. Rev. Lett. **96**, 145006 (2006).
[7]S. Buffechoux *et al.*, Phys. Rev. Lett. **105**, 015005 (2010).
[8]S. Ter-Avetisyan, M. Schnürer, H. Stiel, and P. V. Nickles, J. Phys. D: Appl. Phys. **36**, 2421 (2003).
[9]M. Schüurer, S. Ter-Avetisyan, S. Busch, M. P. Kalachnikov, E. Risse, W. Sandner, and P. V. Nickles, Appl. Phys. B **78**, 895 (2004).
[10]B. Ramakrishna, M. Murakami, M. Borghesi, L. Ehrentraut, P. V. Nickles, M. Schüurer, S. Steinke, J. Psikal, V. Tikhonchuk, and S. Ter-Avetisyan, Phys. Plasmas **17**, 083113 (2010).
[11]V. T. Tikhonchuk, A. A. Andreev, S. G. Bochkarev, and V. Yu. Bychenkov, Plasma Phys. Controlled Fusion **47**, B869 (2005).
[12]V. F. Kovalev, K. I. Popov, V. Yu. Bychenkov, and W. Rozmus, Phys. Plasmas **14**, 053103 (2007).
[13]S. Ter-Avetisyan, M. Schüurer, and P. V. Nickles, J. Phys. D: Appl. Phys. **38**, 863 (2005).
[14]See http://www.exphys.uni-linz.ac.at for stopping power of protons.
[15]S. Ter-Avetisyan, M. Schnürer, D. Hilscher, U. Jahnke, S. Busch, P. V. Nickles, and W. Sandner, Phys. Plasmas **12**, 012702 (2005).
[16]M. V. Ammosov, N. B. Delone, and V. P. Krainov, Sov. Phys. JETP **64**, 1191 (1986).
[17]K. I. Popov, V. Yu. Bychenkov, W. Rozmus, R. D. Sydora, and S. S. Bulanov, Phys. Plasmas **16**, 053106 (2009).
[18]I. Andriyash, V. Yu. Bychenkov, and V. F. Kovalev, JETP Lett. **87**, 623 (2008).
[19]M. Murakami and M. Tanaka, Phys. Plasmas **15**, 082702 (2008).
[20]K. I. Popov, V. Yu. Bychenkov, W. Rozmus, V. F. Kovalev, and R. D. Sydora, Laser Part. Beams **27**, 321 (2009).
[21]K. I. Popov, V. Yu. Bychenkov, W. Rozmus, and L. Ramunno, Phys. Plasmas **17**, 083110 (2010).
[22]A. A. Samarskii, S. A. Gaifulin, A. V. Zakharov *et al.*, in *Problems in Atomic Science and Technology: Problems in Nuclear Physics and Engineering*, edited by E. P. Vashkova (Energoizdat, Moscow, 1983), Vol. 2, p. 38; S. Yu. Guskov, N. V. Zmitrenko, and V. B. Rozanov, JETP **81**, 296 (1995).
[23]I. I. Sobelman, *Introduction to the Theory of Atomic Spectra* (Pergamon, Oxford, 1972); I. I. Sobelman, L. A. Vainshtein, and E. A. Yukov, *Excitation of Atoms and Broadening of Spectral Lines* (Springer-Verlag, Berlin, 1981).